Correspondence to:
G. V. Khazanov,
george.v.khazanov@nasa.gov

Major pathways to electron distribution function formation in regions of diffuse aurora

George V. Khazanov[1] (ID)**, David G. Sibeck[1]** (ID)**, and Eftyhia Zesta[1]** (ID)

[1]Heliospheric Division, NASA/GSFC, Greenbelt, Maryland, USA

Abstract This paper discusses the major pathways of electron distribution function formation in the region of diffuse aurora. The diffuse aurora accounts for about of 75% of the auroral energy precipitating into the upper atmosphere, and its origin has been the subject of much discussion. We show that an earthward stream of precipitating electrons initially injected from the Earth′s plasma sheet via wave-particle interactions degrades in the atmosphere toward lower energies and produces secondary electrons via impact ionization of the neutral atmosphere. These electrons of magnetospheric origin are then reflected back into the magnetosphere along closed dipolar magnetic field lines, leading to a series of reflections and consequent magnetospheric interactions that greatly augment the initially precipitating flux at the upper ionospheric boundary (700–800 km). To date this, systematic magnetosphere-ionosphere coupling element has not been included in auroral research models, and, as we demonstrate in this article, has a dramatic effect (200–300%) on the formation of the precipitating fluxes that result in the diffuse aurora. It is shown that wave-particle interaction processes that drive precipitating fluxes in the region of diffuse aurora from the magnetospheric altitudes are only the first step in the formation of electron precipitation at ionospheric altitudes, and they cannot be separated from the atmospheric "collisional machine" that redistributes and transfers their energy inside the magnetosphere-ionosphere-atmosphere coupling system.

Plain Language Summary It is shown that wave particle interaction processes that drive precipitating fluxes in the region of diffuse aurora from the magnetospheric altitudes are only the first step in the formation of electron precipitation at ionospheric altitudes, and they cannot be separated from the atmospheric "collisional machine" that redistributes and transfers their energy inside the magnetosphere-ionosphere-atmosphere coupling system.

1. Introduction

The aurora is considered one of the most important and fundamental phenomena in space physics. Its occurrence is related to the interaction of the solar wind with the Earth's magnetosphere and the associated magnetosphere-ionosphere-thermosphere coupling processes. Among the different types of aurora, the diffuse aurora is the most powerful one, delivering about 75% of the auroral energy that enters the ionosphere [*Newell et al.*, 2009]. Unlike the discrete aurora, the diffuse aurora is a large-scale auroral phenomena that occurs over a broad range of latitudes and is primarily caused by the precipitation of low-energy (0.1–30 keV) electrons originating in the central plasma sheet. The diffuse aurora produces an auroral oval shaped by the level of geomagnetic activity; the oval's location maps along magnetic field lines to the plasma sheet. Both ions and electrons precipitate in the diffuse aurora, although the average integral number flux of the precipitating auroral ions is typically 1 to 2 orders of magnitude less than that of the precipitating auroral electrons [*Hardy et al.*, 1989].

It is well known that pitch angle diffusion generates diffuse aurora through cyclotron resonances [*Kennel and Petschek*, 1966], although the location of this wave-particle interaction process remains a subject of debate. Previous theoretical studies have indicated that electron cyclotron harmonic (ECH) and whistler mode chorus waves are two distinct classes of magnetospheric plasma waves, but it has not been possible to determine which makes the most important contribution to low-energy flux enhancement. Based on an analysis of in situ wave observations [*Meredith et al.*, 2009] and Fokker-Planck diffusion calculations, *Thorne et al.* [2010] seem to resolve this long-standing controversy and found that scattering by chorus can remove most electrons as they drift around Earth's magnetosphere. This scattering process explains the observed pancake pitch angle distributions [*Meredith et al.*, 2009] and can account for the global morphology of the diffuse aurora [*Petrinec et al.*, 1999; *Newell et al.*, 2009; *Su et al.*, 2009, 2010].

All of the aforementioned electron precipitation studies at auroral latitudes are based on the assumption that pitch angle diffusion from the trapped zone to the loss cone is the only source of such precipitation into the atmosphere-ionosphere system. These previous studies do not consider the contribution of magnetosphere-ionosphere (MI) coupling processes in the formation of the electron distribution function at the MI boundary (700–800 km) (see papers by *Khazanov et al.* [2015a, 2015b] for a detailed discussion of the role of MI coupling processes in the formation of electron distribution function in the diffuse aurora). They correctly identify that the initial precipitation into the atmosphere results from pitch angle scattering of plasma sheet electrons into the loss cone by different kinds of wave-particle interaction processes; this can be considered a purely magnetospheric process. However, the interaction of these precipitating primary magnetospheric electrons with the neutral atmosphere also leads to the production of secondary electrons ($E < 500$–600 eV), as well as the degradation and reflection of electrons that initially were trapped in the Earth's plasma sheet. While the ECH and whistler mode chorus waves are often only considered to be the drivers of the primary precipitating electrons, they can also interact with the secondary as well as the degraded and reflected electrons (initially injected from the magnetosphere) as they travel back through the magnetosphere to the magnetically conjugate ionosphere [*Khazanov et al.*, 2015b]. In addition, it is believed that the parallel electric field is absent in regions of diffuse aurora and that ECH and whistler mode chorus waves drive plasma sheet electron precipitation simultaneously in both magnetically conjugate regions. The last statement makes the MI coupling element of the formation of the downward electron fluxes in the auroral regions even more strongly pronounced. The analysis of all these transport and scattering processes involved in the formation of electron fluxes must therefore begin by considering the magnetosphere and ionosphere as a single system, although they have historically been separated.

As shown by *Khazanov et al.* [2014], about 15–40% of the energy of precipitating electrons returns back to the magnetosphere and the conjugate ionospheric point of an auroral magnetic field line, depending on the energy spectra of the initial precipitation in the regions of diffuse aurora. Previous research by *Khazanov et al.* [2014] considered both magnetically conjugate ionospheric regions, with the electron precipitation in each region prescribed in the energy range above of 600 eV and applied at both ionospheric boundaries (800 km). *Khazanov et al.* [2015a] followed up on this work and considered a similar scenario with a new modification of the ionospheric boundary conditions that takes into account the multiple reflections of electrons initially injected from the magnetosphere. They also found that the MI coupling element plays an extremely important role in the formation of the electron fluxes that precipitate into the ionosphere.

Like *Khazanov et al.* [2015b], we will initiate the electron precipitation processes via wave-particle interaction (WPI) processes, thereby removing the need for ionospheric boundary conditions at 800 km. This allowed us to account for effects of ECH and whistler mode chorus wave interaction with the Earth's plasma sheet on the initial primary electron precipitation into both magnetically conjugated atmospheres. To do this, *Khazanov et al.* [2015b] set up the pitch angle boundary conditions for magnetospheric electrons with energies above 600 eV at the loss cone and assumed that there is no communication between the initially trapped magnetospheric electrons and the electrons with the same energies that return through the loss cone after reflection and degradation in both magnetically conjugated regions. Now we are removing these assumptions by allowing magnetospheric electrons reflected by the atmosphere to communicate back and forth between the loss cone and trapped zones as they travel back to the magnetosphere and to the magnetically conjugate ionospheric regions. We also naturally demonstrate the role of the multiple atmospheric electron reflections that were introduced phenomenological by *Khazanov et al.* [2015a] and the role of magnetically conjugate atmospheric regions based on the first principles of the solution of the Landau-Boltzmann equation throughout the entire MI coupling system.

This paper is organized into the following sections: the methodology, physical scenario, and mathematical formalism of the simulations are described in section 2. All of our results are discussed in sections 3 and 4, and finally, section 5 presents the summary of this paper.

2. The Methodology and Simulation Scenario

The methodology used in this paper is based on the nonsteady state superthermal electron transport (STET) code that was initially developed by *Khazanov et al.* [1993] for superthermal electron (SE) transport in the plasmasphere. This code was further generalized for ionosphere-magnetosphere coupling studies
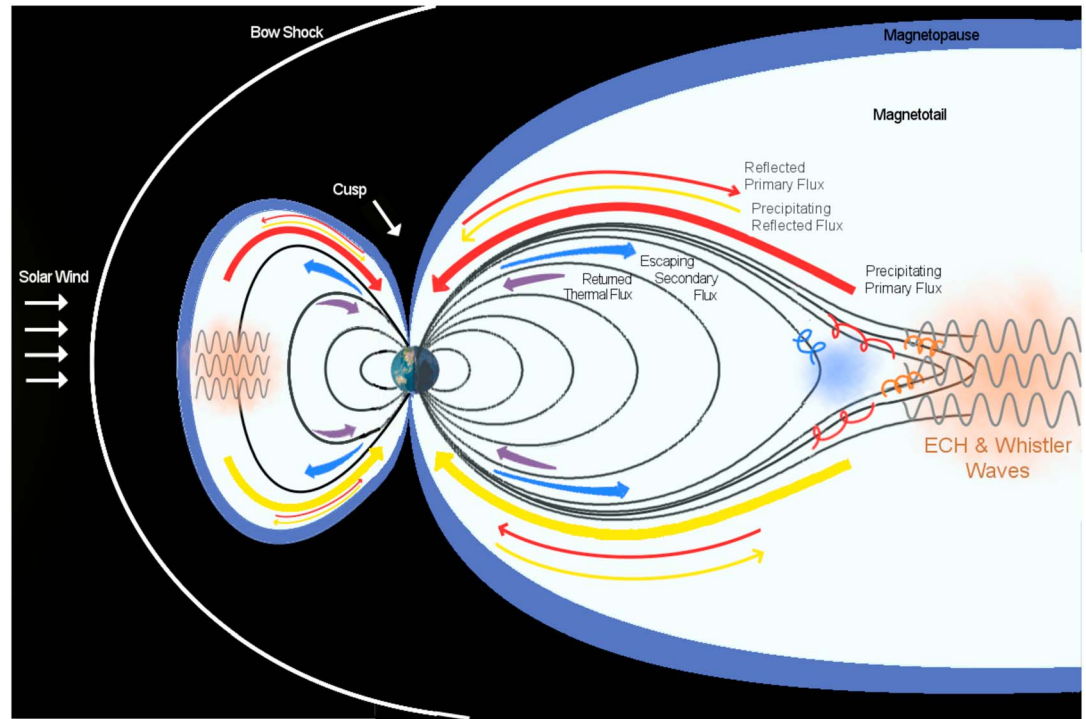
Figure 1. Scenario of MI coupling simulations by STET code.

[*Khazanov and Liemohn*, 1995], the global transport of SE [*Khazanov et al.*, 1996], and to study relativistic beam injections in space plasmas [*Khazanov et al.*, 1999]. The STET model to be used in this paper has been discussed in great detail by *Khazanov* [2011] and presented in more recent studies by *Khazanov et al.* [2014, 2015a, 2015b]. To avoid repetition, we refer the reader back to those papers for full details. However, a brief description is provided here.

As in the papers by *Khazanov et al.* [2014, 2015a, 2015b], the starting point for our superthermal electron MI coupling problem is the Boltzmann-Landau kinetic equation presented by *Khazanov* [2011]. Following *Khazanov* [2011], this equation can be written as follows:

$$\frac{1}{v}\frac{\partial\Phi}{\partial t} + \mu\frac{\partial\Phi}{\partial s} - \frac{1-\mu^2}{2}\left(\frac{1}{B}\frac{\partial B}{\partial s} - \frac{F}{E}\right)\frac{\partial\Phi}{\partial\mu} + EF\mu\frac{\partial}{\partial E}\left(\frac{\Phi}{E}\right) = Q + \langle S\rangle,\tag{1}$$

where $\Phi = 2Ef/m2$ is the SE flux, f is the electron distribution function, v is SE velocity, t is time, s is the distance along the field line, E is the particle energy, and μ is the cosine of the pitch angle. F includes the inhomogeneity of the geomagnetic field, B, as well as other forces. Q is the SE source term, and $\langle S\rangle$, which includes collision integrals, represents interactions with thermal electrons and ions, scattering with neutral particles, and wave-particle interactions. All these terms have presented in previous papers by *Khazanov et al.* [2014, 2015a, 2015b] and will not be repeated here. The electric field in kinetic equation (1) is expressed through the total gradient of the thermal electron pressure.

Figure 1 illustrates our simulation scenario that has been discussed in details by *Khazanov et al.* [2015a, 2015b] and will not be repeated here again. Further, as has been discussed by *Khazanov et al.* [2015a, 2015b], it is convenient to change variables in (1) from (μ, s) to (μ_0, s), where

$$\mu_0(s) = \frac{\mu}{|\mu|}\sqrt{1 - \frac{B_0}{B(s)}\left(1 - \mu^2\right)},\tag{2}$$

with B_0 and μ_0 denoting the magnetic field strength and the cosine of the pitch angle at the magnetic equator of the flux tube. After the change of variables $\Phi(\mu_0, s)$ now becomes a slowly varying function with s that
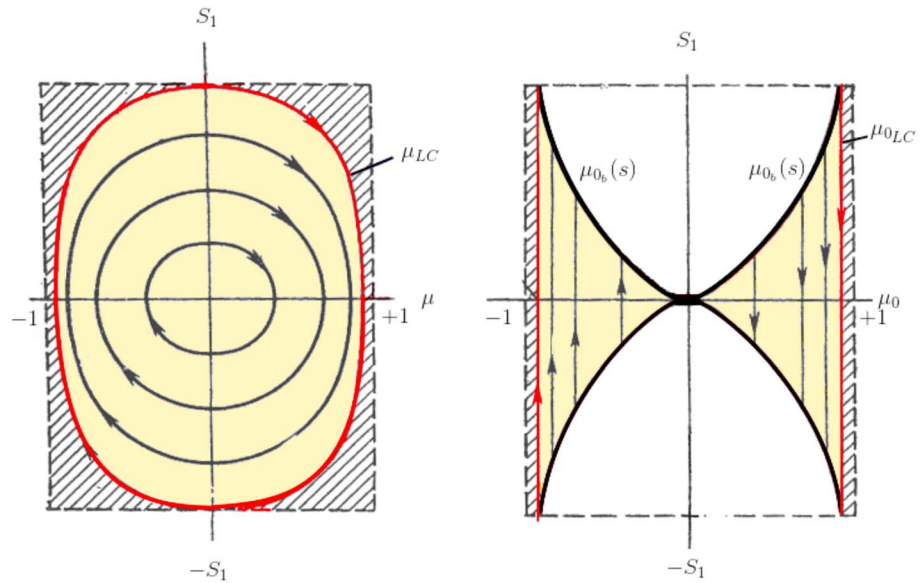
Figure 2. Regions where we solve the kinetic equation (1) using different pitch angle variables (2).

greatly reduces computational effects associated with approximating errors in the derivatives (see *Khazanov* [2011] for the details). Figure 2, taken from the paper by *Khazanov et al.* [2015b], represents the regions for the solution of kinetic equation (1) using different pitch angle variables connected by (2).

As noted in section 1, *Khazanov et al.* [2015b] initiated electron precipitation from the magnetosphere to ionosphere via ECH and whistler waves interacting with the Earth's plasma sheet. The boundary conditions were set up in velocity space above 600 eV and at the loss cone (see red lines in Figure 2). It was also assumed that there is no communication between the initially trapped magnetospheric electrons (yellow region in Figure 2) and the electrons with the same energies that return through the loss cone (shaded area at the same figure) after reflection and degradation in both magnetically conjugated regions. Now we are removing these assumptions by allowing magnetospheric electrons reflected by the atmosphere to communicate back and forth between the loss cone and trapped zones as they travel back to the magnetosphere and to the magnetically conjugate ionospheric regions. We also naturally demonstrate the role of the multiple atmospheric electron reflections that were introduced by *Khazanov et al.* [2015a] and the role of magnetically conjugate atmospheric regions based on first principle solutions of the Landau-Boltzmann equation for the entire MI coupling system.

Like *Khazanov et al.* [2015b], we assume that trapped electron fluxes are isotropic and their energy distribution is consistent with a typical Maxwellian-like energy distribution in the region of diffuse aurora [*Rees*, 1989]:

$$\Phi_{\text{trap}}(E) = AE \exp(-E/E_0). \tag{3}$$

Here A is the normalization factor and E_0 is the characteristic energy of the trapped plasma sheet electrons. To be consistent with the paper by *Khazanov et al.* [2015b], we have chosen in $A = 10^3$ and $E0 = 1$ KeV. We also assume these parameters to be the same at L shells of 4.6 and 6.8 and apply (3) for the energy range between 600 eV and 10 KeV. The specific wave parameters are presented in Table 1 and are within the range of the observed wave database from CRRES [*Meredith et al.*, 2009].

Table 1. Plasma and Waves Parameters in the Earth's Plasma Sheet

Parameters	B_0 (nT)	n_c (cm^{-3})	T_c (eV)	UBC (pT)	LBC (pT)	ECH (mVm^{-1})
L = 4.6	312	21.5	4.0	10	10	1.0
L = 6.8	92.5	12.0	10	10	10	1.0

3. Loss Cone—Trap Zones Communication

Now without further ado, we present the new solution without the previous restrictions mentioned above for both the initially injected and secondary electrons and compare our new results with our previous calculations. For consistency with previous work, we initiate SE injection into the loss cone with the energies of 600–10,000 eV and consider Maxwellian-like spectra for the plasma sheet electrons (3).

Figure 3 compares downward and upward SE fluxes at an altitude of 800 km calculated by the new and old approaches. These fluxes are presented for two different L shells, 4.6 and 6.8, and are calculated using *the same intensities* of ECH and whistler modes for *the different magnetospheric locations*. This plot also shows the ratio between old and new results (the third window in the first row) as well as the ratio of upward and downward fluxes (the third window in the second row). The lines styles that are chosen here clearly demonstrate all the differences between our previous and current results that are discussed below.

As mentioned in the model description section (see also Table 1), the amplitude of the magnetic field fluctuations for the lower bounded chorus (LBC) and upper bounded chorus (UBC) whistler waves are taken to be 10 pT and for ECH waves a value of 1 mVm^{-1} is used. Values at both L shells are identical. These values are within the range of observed wave database from CRRES [*Meredith et al.*, 2009; *Ni et al.*, 2011a, 2011b] and produce quite different pitch angle diffusion coefficients for L = 4.6 and 6.8 that are presented in Figures 1 and 2 of recently published paper by *Tripathi et al.* [2016]. As a result, the intensities of downward and upward electron fluxes that are calculated at the ionospheric altitudes are noticeably different for the both old and new approaches.

As expected, the new formulation of the STET code that takes into account communication between the loss cone and trapped zone, as shown on Figure 2, leads to enhanced SE fluxes throughout the entire energy range as presented in Figure 3. Now the MI coupling SE process becomes more complicated. The SEs that initially were in the Earth's plasma sheet and experienced WPI in this area move into the loss cone and precipitate into both magnetically conjugate ionospheres as long as wave activity exists. In fact, according to *Horne et al.* [2003], *Meredith et al.* [1999, 2009], and *Li et al.* [2013], ECH, LBC, and UBC waves emissions can last for several hours, and, as a result, we can consider the formation of SE fluxes to be a steady state process [*Khazanov et al.*, 2015a, 2015b]. These initially precipitating electrons with energies from 600 eV to 10 KeV interact with the neutral atmosphere via different kinds of elastic, nonelastic, and ionization collisional processes, leading them to reflect upward, degrading them toward lower energies and producing secondary electrons. All these electrons can partially escape back to the magnetosphere, traveling through the same region of wave activity, and interact with ECH and whistler mode waves. As these electrons travel back to the magnetically conjugate ionospheric regions and pass through the regions of ECH and whistler modes activity near the geomagnetic equator, they can be partially trapped back into the plasma sheet, only later to come back to the loss cone area and precipitate into both ionospheres, eventually enhancing the downward primary precipitating electron flux.

The quantitative enhancement of downward and upward fluxes seen by comparing the new and old STET results shown in the third window of the first row in Figure 3 is quite noticeable. On average, for the given level of ECH and whistler wave activity, it is about 30%. In the transitional energy range between the primary (E > 600 eV) and secondary (E < 600 eV) electrons the magnitude of the differences between the new and old results depends on L shell position and varies differently for the downward and upward fluxes, but with some slight fluctuations in these ratios due to the corresponding resonance structure of the pitch angle diffusion coefficients for the ECH and whistler waves [*Khazanov et al.*, 2015b; *Tripathi et al.*, 2016].

The third window of the second row in Figure 3 presents ratios of new to old results for the downward and upward fluxes. Compared to the ratios between the new and old fluxes themselves (the third window of the first row), these variations are much smaller because the new STET algorithm, as described above, proportionally increases both downward and upward fluxes. As one can see from this window, the difference between fluxes up and down is a function of energy and, for the given magnetospheric parameters, maximizes around 20 eV for both L shells, 4.6 and 6.8.

Figure 4 shows the energy distribution of SE for different pitch angles at L = 4.6 and L = 6.8 in the magnetosphere at the geomagnetic equator. These distributions are presented for pitch angles of 0°, 2°, 4°, 20°, 30°,
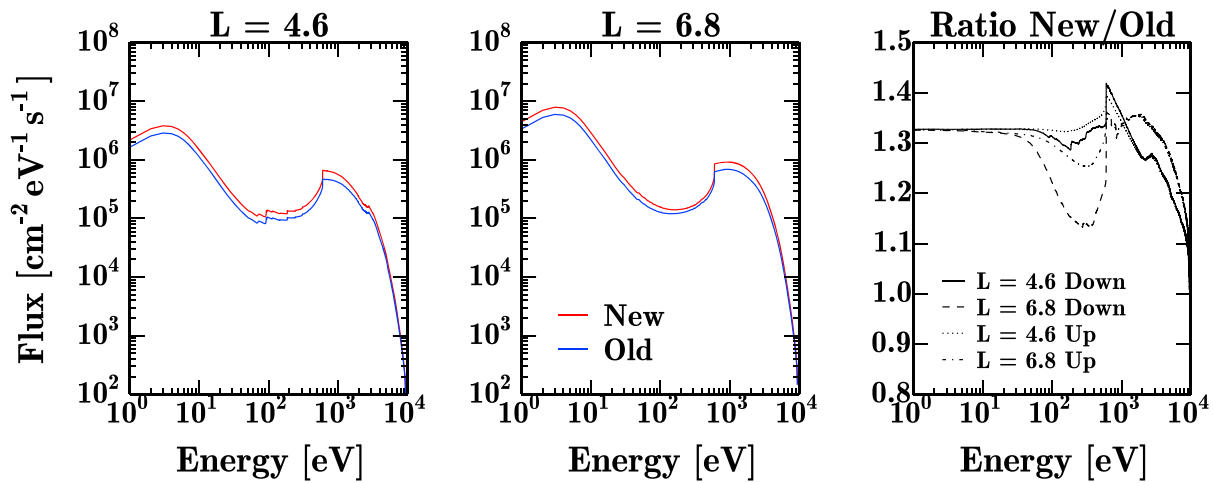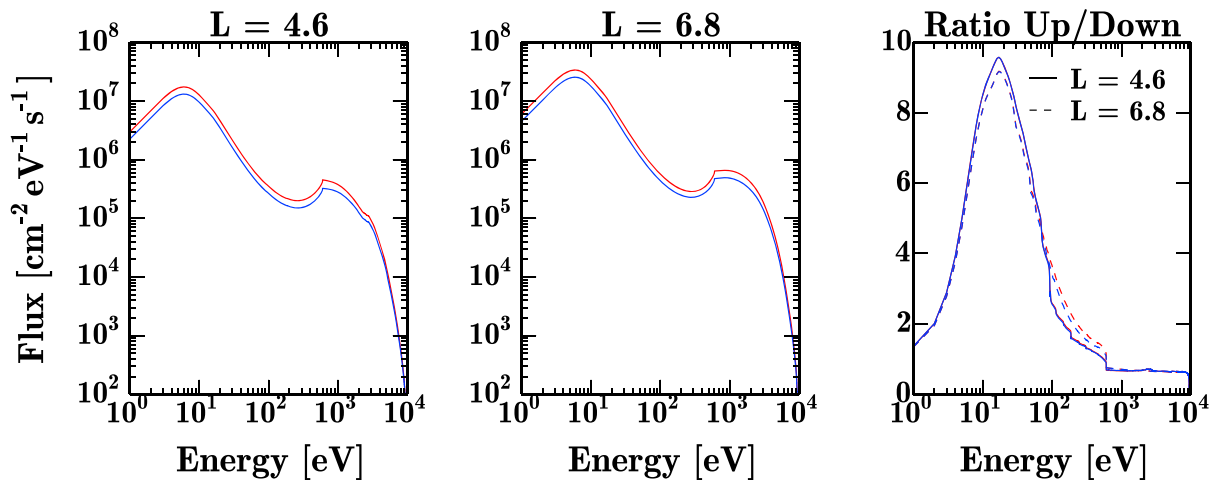
Figure 3. Compare old and new simulations scenarios for downward fluxes.

40°, 60°, 75°, and 90°, respectively. Selected pitch angles correspond to different electron distribution function positions with respect to the loss cone and trapped zones. The energy spectra in the first row of Figure 4 show electrons with 0° pitch angles that are in the loss cone, particles with 2°, and 4° pitch angles, for both $L = 4.6$ and $L = 6.8$ that lie close to the loss cone boundary (red line in Figure 2). Correspondingly, the second and the third rows of this plot show pitch angle ranges that are deep inside, but in different positions within the trapping zone.

The results presented in Figure 4 resemble those in Figure 3. The inclusion of communication between the loss cone and trapped zones in the energy range above 600 eV leads to the total flux enhancement. However, the specific energy flux redistribution depends on energy and pitch angle. For example, starting from pitch angles above 20°, and energies more than about 100 eV, for both $L = 4.6$ and $L = 6.8$, the old calculations (blue lines) dominate over the new ones. Apparently, this dependence corresponds to the complicated behavior of the pitch angles diffusion coefficients, D_{aa}, presented in Figures 4–7 of the paper by *Khazanov et al.* [2015b]. In the new approach, at these pitch angles and energies, the pitch angle diffusion that pushes electrons toward the loss cone dominates over the pitch angle diffusion in the opposite direction, toward the trapped zone.
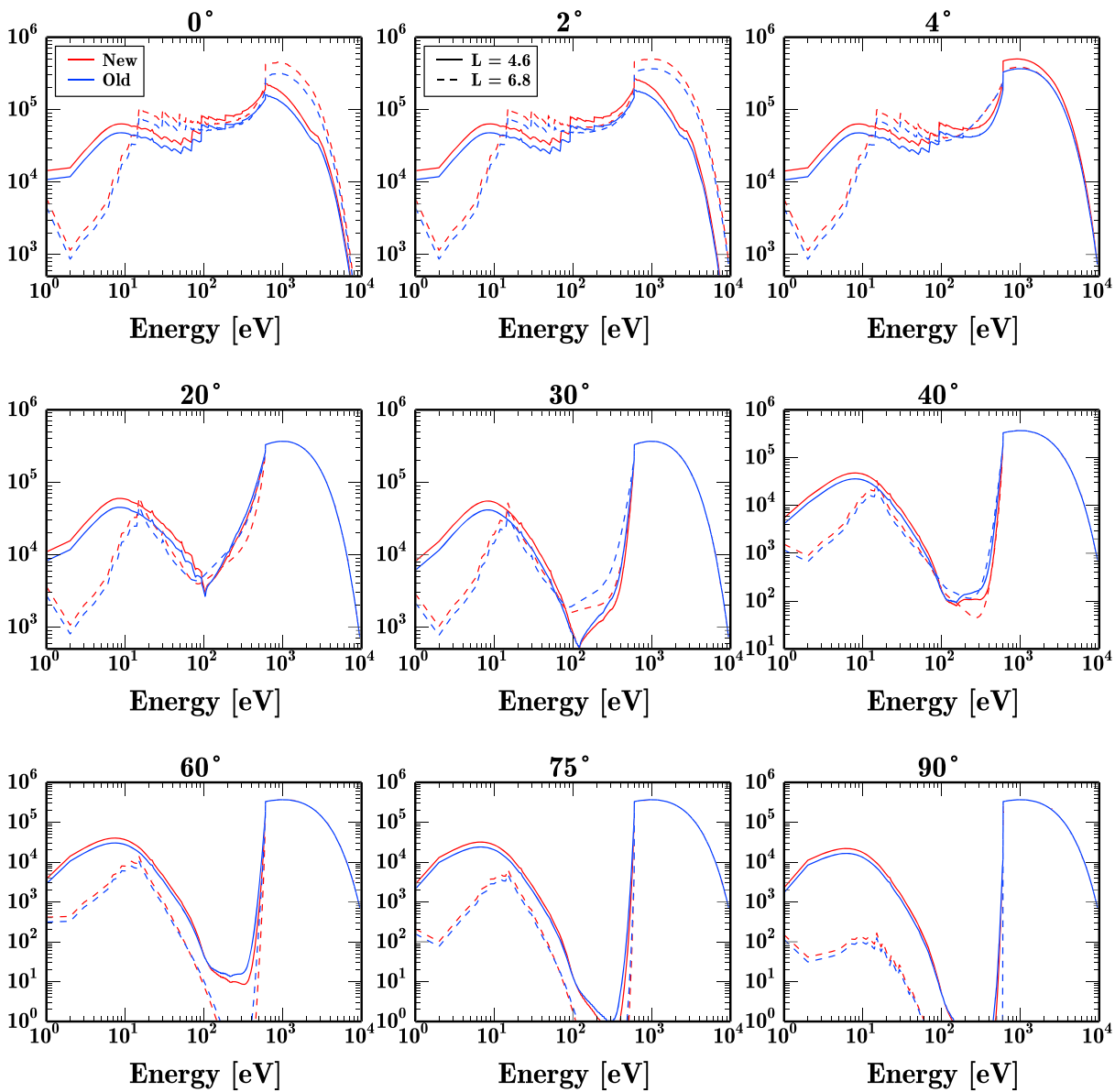
Figure 4. Compare old and new simulations scenarios for energy fluxes at the magnetic equator for the different pitch angles.

Figure 5 shows pitch angle distributions for different energies in the equatorial plane of the magnetosphere for the case of symmetric precipitation into the Northern and Southern Hemispheres and $L = 4.6$ and 6.8. All notations at this figure are consistent with those for Figures 3 and 4. Because of the symmetric precipitation, the figure shows only the electron fluxes moving from the northern to the southern conjugate ionosphere. Pitch angle scales for these plots different for energies of 10, 20, 30, 100, 200, and 500 eV in the first and second rows compared to those for 1, 2, and 5 keV in the third row. The new simulation scenario leads to the flux enhancements for the energies presented in the first and third rows that, correspondingly, represent the low- and high-energy spectra of the electron distribution function. The pitch angle distributions in the intermittent energy range at 100, 200, and 500 eV, shown in the second row of the Figure 5, exhibits a more complicated behavior, similar to that for 100 eV energies presented in Figure 4. Here electron fluxes from the new simulation scenario dominate over the old one only in the loss cone or close to it on the trapped zone side. The explanation for this is very similar to that for Figure 4; in the new approach, at these pitch angles and energies, the pitch angle diffusion that pushes electrons toward the loss cone dominates over the pitch angle diffusion in the opposite direction, toward the trapped zone. That is why, for these energies, this leads to the flux depletion in the new simulation scenario.
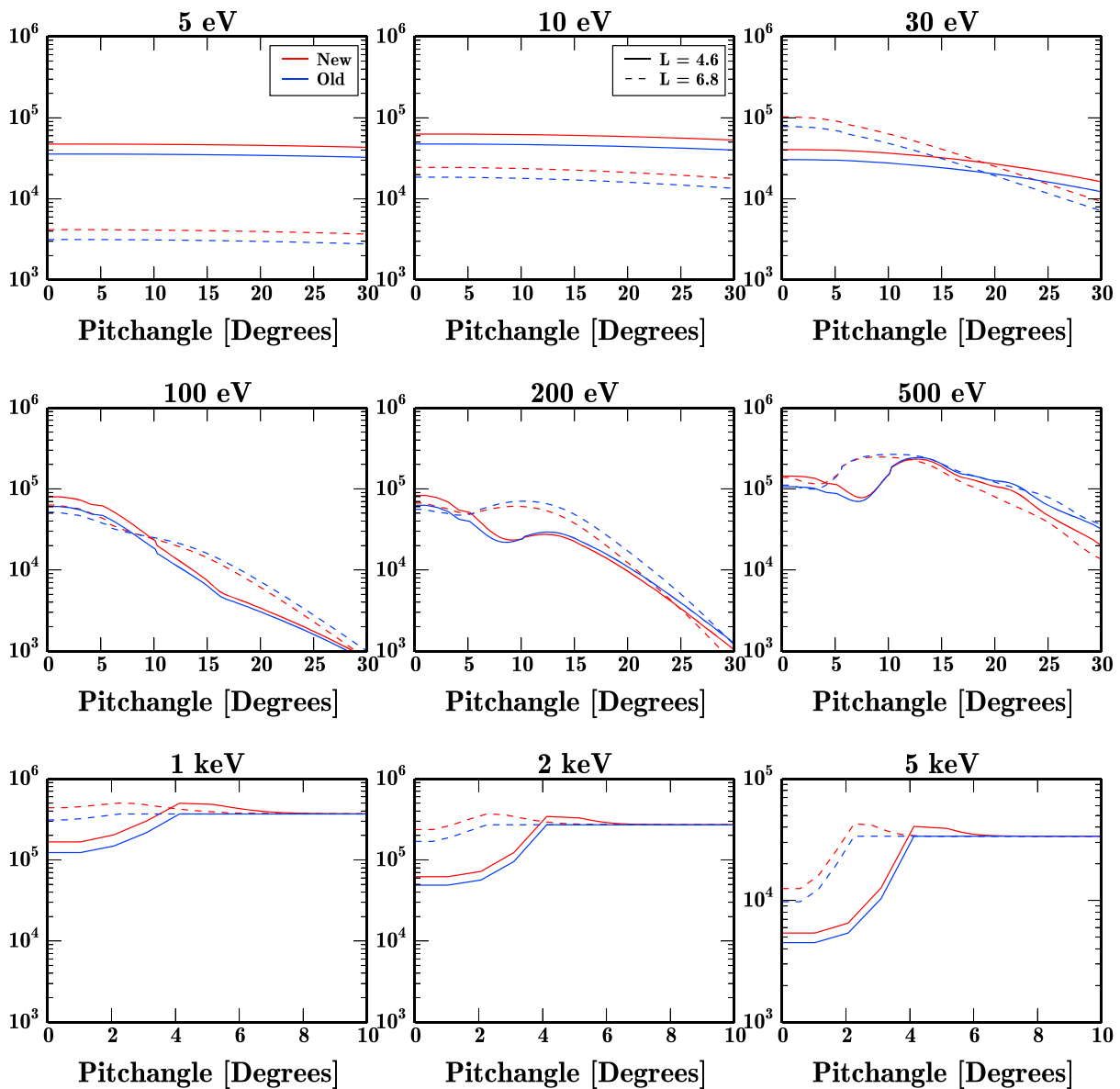
Figure 5. Pitch angle distribution for the different energies at the geomagnetic equator: compare old and new simulations scenarios.

4. The Role of the Conjugate Ionosphere and Multiple Reflections

As noted in section 1, the present study targets the MI coupling element in the formation of electron fluxes in the regions of diffuse aurora. From now on, we will be presenting only the STET model results based on the newly developed algorithm that takes into account communication between the loss cone and trapped zones (Figure 2) in both directions. Numerous STET code simulations were conducted to investigate the effects of MI coupling on the electron distribution function in the regions of diffuse aurora. Specifically, we want to address the role of the magnetically conjugate ionospheric region and multiple magnetically conjugate atmospheric reflections in the formation of precipitating electron fluxes in the regions of diffuse aurora. Table 2 lists notations for the various simulation scenarios presented in this section that will help us to understand the role of the major pathways to electron distribution function formation in this particular region of the space plasma.

We must emphasize that considering only electron precipitation driven by ECH and/or whistler waves in the Earth's plasma sheen is not a complete picture and that the role of the MI coupling element in the formation must be taken into account. As we will show, WPI processes that drive precipitating fluxes in the region of

Table 2. STET Simulation Scenarios

Notation	Description of MI Coupling Simulation Scenario
All	Two magnetically conjugated ionospheric regions are coupled together with communication between the loss cone and trapped zones.
NoCong	The Southern Hemisphere is completely disconnected from the simulation.
NoRe12	Case like All, but no elastic scattering processes are allowed in the Northern (1) and Southern (2) Hemispheres.
NoRef1	Case like All, but no elastic scattering processes are allowed in the Northern (1) Hemisphere.
NoRef2	Case like All, but no elastic scattering processes are allowed in Southern (2) Hemisphere.
Nolono	Both magnetically conjugated regions are completely disconnected from the magnetosphere.

diffuse aurora from magnetospheric altitudes are only the first step in the formation of electron precipitation at ionospheric altitudes, and they cannot be separated from the atmospheric collisional machine that redistributes and transfers their energy inside MI coupling system.

Figure 6 presents omnidirectional electron fluxes in the Northern Hemisphere at ionospheric altitudes ranging from 150 km to 800 km. The first row of this plot corresponds to $L = 4.6$ and the second to $L = 6.8$. Note that to calculate these fluxes for the different L shells, we used identical wave activities and plasma sheet data as described in section 2. Nevertheless, similar to previous work by *Khazanov et al.* [2015b], precipitation is stronger at $L = 6.8$. This is due to the greater efficiency of WPI processes at larger distances. The first window in each row corresponds to the case when all processes that are listed in Table 2 are taken into account (All) and the second one to the case when the southern magnetically conjugate region was completely disconnected from the MI coupling energy interchange (case NoCong in Table 2). Figure 6 (right windows) also shows the ratios of omnidirectional fluxes at different L shells and indicates that magnetically conjugate ionospheric regions have a dramatic impact on the electron precipitation and must be taken into account in all modeling networks that predict the effects of electron precipitation phenomena at ionospheric altitudes. As one can conclude from the A/B ratios presented at this figure, the contribution of the magnetically conjugate ionosphere to the omnidirectional fluxes formation at ionospheric altitudes is a function of the L shell position, the intensity of the activity of ECH and whistler waves, the character of the electron energy spectra in the Earth's plasma sheet, and the local magnetospheric environment where the WPI takes place.

When we studied the role of the magnetically conjugate ionosphere in the production of diffuse auroral fluxes (see also Figures 7–9 and case NoCong in Table 2), the southern conjugate ionosphere was complete disconnected from our simulations. Such an asymmetry in the production of the diffuse aurora also follows from the ground-based conjugate observation presented by *Sato et al.* [2016].

To continue our discussion regarding the role of MI coupling processes in the formation of SE fluxes in the regions of diffuse aurora, we present the different STET code simulation scenarios listed in Table 2 and shown at Figures 7–9. Please note that the colors for all these figures are intentionally coordinated.

Figure 7 shows downward fluxes at an altitude of 800 km in the Northern Hemisphere (region 1) for $L = 4.6$ (left window) and $L = 6.8$ (right window). We compare these fluxes for different MI coupling conditions with respect to the Southern Hemisphere (region 2) as well as with the completely decoupled ionosphere and magnetosphere systems as indicated in Table 2. When analyzing data presented in Figure 7, it is convenient to separate initially injected electrons of magnetospheric origin, energies $E > 600$ eV, from secondary electrons energies, $E < 600$ eV. For example, for the energies $E > 600$ eV, turning off the magnetically conjugate region in southern ionosphere (NoCong) leads to exactly the same effect as if one ignores elastic reflections in region 2 (NoRef2). However, comparing the same simulations for the energies below 600 eV, we note some differences in energy spectra behavior in a 100 eV energy range. The enhanced downward fluxes for these energies results from the interaction of precipitating plasma sheet electrons in region 2 with the neutral atmosphere and the production of secondary electrons that easily escape to the Northern Hemisphere without any elastic collision scattering by neutral and plasma particles.

The elastic atmospheric collisional processes represent the ionospheric portion of the MI coupling phenomena and work differently with respect to the Northern and Southern Hemispheres. Continuing the discussion of Figure 7, there is another simulation scenario, NoRef1, when elastic collisional processes were ignored only in the Northern Hemisphere. In this case the energy spectra have a more complicated structure, and, in
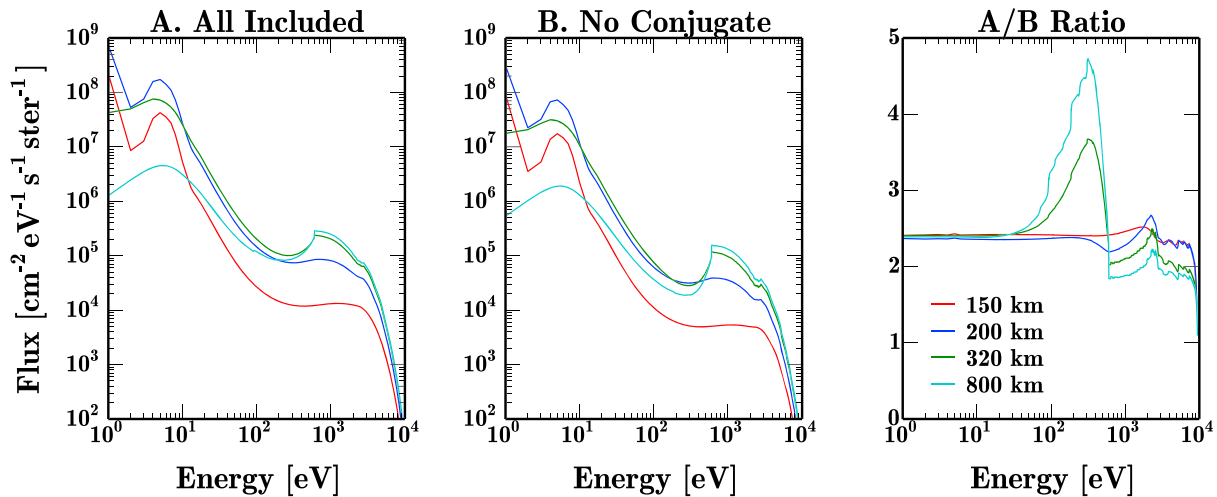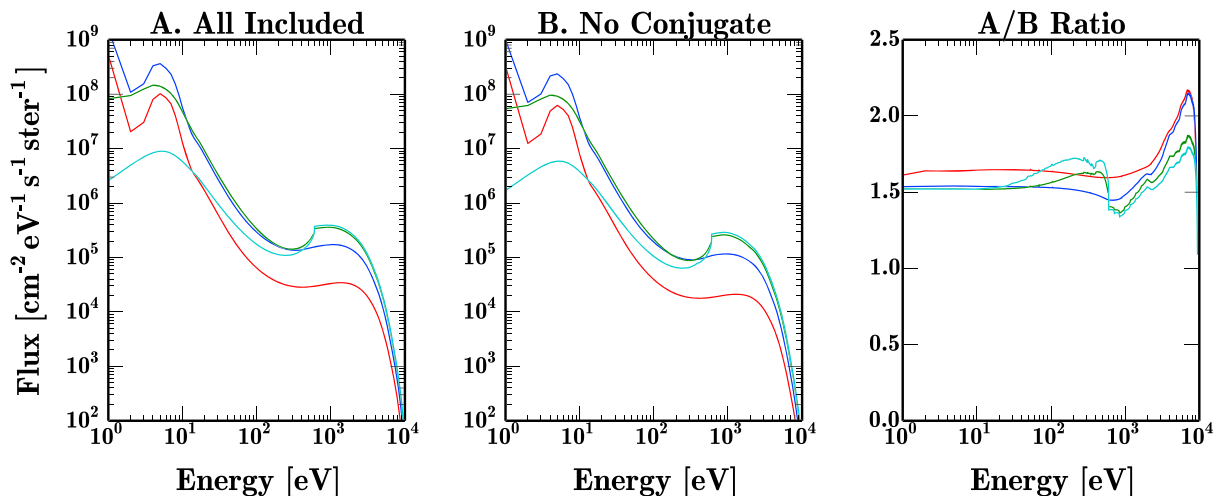
Figure 6. Omnidirectional fluxes at the ionospheric altitudes that show the role of magnetically conjugate ionospheres at $L = 4.6$ and $L = 6.8$.

general, the total secondary fluxes that are coming down to the Northern Hemisphere are smaller. In this case the elastic collisional processes were presented in the southern ionosphere, and they decrease the number of the secondary electrons that were escaping up from the region 2 and coming down to region 1 in the Northern Hemisphere.

All other cases that are shown in Figure 7 are quite easily explained. Ignoring elastic scattering in both magnetically conjugate ionospheric regions (NoRe12) leads to a disconnection of MI coupling process in the energy range of $E > 600$ eV and produces results that correspond to the case of NoIono. Because of this, it also drastically reduces the production of the secondary electrons, $E < 600$ eV, and, as a result, causes a depletion of the secondary electron fluxes.

Let us consider some of the details of NoCong simulation scenario. Referring to Figure 1 of this manuscript, the NoCong case has no "precipitating primary flux" into the Southern Hemisphere as labeled on this figure by large yellow arrow. In this case we only allow all communications between Northern Hemisphere and magnetosphere. The downward electron fluxes that come into the region 1 result from the precipitating primary flux into the Northern Hemisphere as indicated by the large red arrow in Figure 1 and multiple reflections (shown in this figure by smaller outgoing red arrows) between the northern ionosphere and
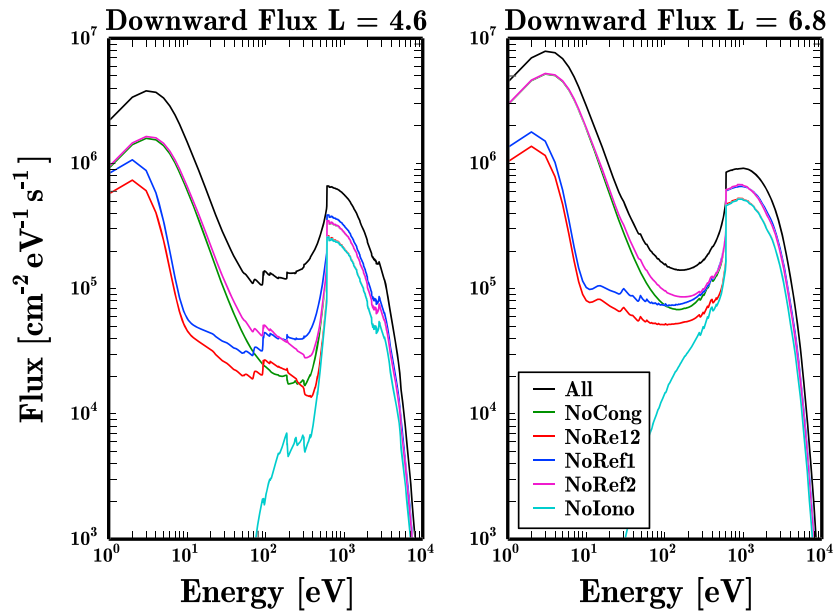
Figure 7. Downward electron flux from 1 eV to 10 keV at 800 km for $L = 4.6$ and $L = 6.8$ calculated for six different MI scenarios as described in the text.

magnetosphere. However, we are not allowing these reflected fluxes to precipitate into the Southern Hemisphere. When these electrons are reflected back from region 1 and escape to the magnetosphere, they just circulate multiple times between the loss cone and trap zones in the magnetosphere and return back to the northern ionosphere. That is why downward fluxes in this case are bigger than in the simulation scenario of NoIono, when there are no communications at all between the both magnetically conjugate ionospheres and magnetosphere.

In general, there are some other minor differences in the behavior of the energy spectra for the $L = 4.6$ and $L = 6.8$ that are defined by the pitch angle diffusion coefficients, D_{aa}, presented in Figures 4–7 of *Khazanov et al.* [2015b] that are omitted from our discussion above. In particular, the bumpy shape of the SE fluxes presented in Figure 7 of this paper is due to the bumpy behavior of the pitch angle diffusion coefficients
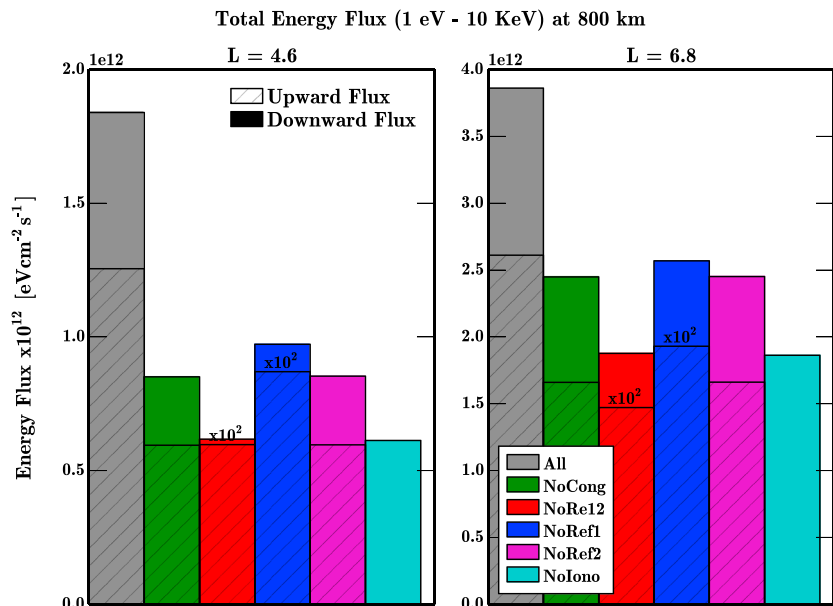

Figure 8. Upward and downward integrated electron fluxes calculated for the same scenarios as Figure 7.
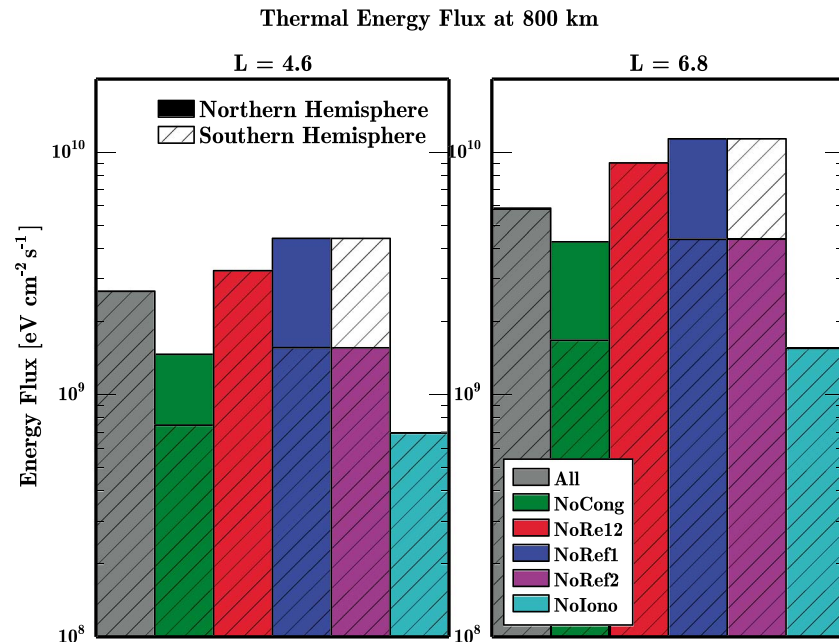
Figure 9. The electron thermal fluxes from the magnetosphere at *L* = 4.6 and *L* = 6.8 calculated for six different MI scenarios as described in the text.

[*Khazanov et al.*, 2015b]. Also, one should keep in mind that in order to be consistent with all of previous diffuse aurora studies, the primary spectrum injected into the ionosphere (3) decreases sharply below 600 eV. That, and the 1 eV energy resolution in the STET code, cause some of the sharp energy gradients presented above in the energy spectra of superthermal electrons. All these peculiarities, however, have no influence at all regarding the role of the MI coupling processes in the formation of electron distribution function in the regions of the diffuse auroras.

Figure 8 shows the total downward (solid bars) and upward (dashed bars) directional energy fluxes at 800 km altitude integrated from 1 eV to 10 keV for *L* = 4.6 (left) and *L* = 6.8 (right). These energy fluxes are calculated for the six scenarios listed in Table 2, and this histogram further demonstrates the great role of MI coupling processes in the formation of SE fluxes that precipitate into the upper atmosphere. As we noted above, for the different L shells, we used identical activities of wave and plasma sheet data as described in section 2 of this paper. Nevertheless, similar to Figure 7, and previous work by *Khazanov et al.* [2015b], precipitation is stronger at *L* = 6.8 due to the greater efficiency of WPI processes at larger distances.

To emphasize the role of MI coupling processes in the formation of downward energy and/or particle fluxes in the regions of diffuse aurora, compare the corresponding cases for NoIono and All presented in Figure 8. The difference between these two scenarios in the calculated electron energy fluxes is 300% for *L* = 4.6 and more than 200% for *L* = 6.8. Therefore, considering only electron precipitations that are driven by ECH and/or whistler waves in the Earth's plasma sheet is not a complete picture, and the MI coupling element in the formation *must* be taken into account. As was shown by *Khazanov et al.* [2015a], when the mean energy increases, the effect of MI coupling process in the formation of electron distribution function in the regions of diffuse aurora becomes even stronger. It is also expected that taking into account more realistic electron kappa distribution in the Earth's plasma sheet measured by Time History of Events and Macroscale Interactions during Substorms mission and presented by *Runov et al.* [2015] would lead to a further increase in the role of the MI coupling processes and, as a result, increase the precipitated electron fluxes.

Finally, Figure 9 presents the thermal energy flux at 800 km altitude entering the Northern and Southern Hemispheres from the magnetosphere, as calculated for the different MI coupling precipitated scenarios in Table 2. These thermal electron fluxes returning to the ionosphere were discussed in section 2 and are shown by purple arrows labeled returned thermal flux in Figure 1. Thermal fluxes form when secondary electrons escaping from the ionosphere are degraded via Coulomb collisions in the magnetosphere. As the secondary electrons ($E < 600$ eV) escape back to the magnetosphere (see blue arrows in Figure 1), they can become

trapped in the magnetosphere via WPI and Coulomb collisional processes and deposit their energy into the thermal magnetospheric electrons. For details of these processes, refer to *Khazanov et al.* [2014].

The solid bars in Figure 9 correspond to the thermal energy fluxes entering the Northern Hemisphere, while the dashed bars indicate the thermal energy fluxes entering the Southern Hemisphere. The left window in this plot represents results for $L = 4.6$ and the right one for $L = 6.8$. The intensities of the thermal electron energy fluxes that entering the ionosphere are very small compared to the total SE energy fluxes shown in Figure 8. However, they play an extremely important role in the formation of the electron plasma temperature in the plasmasphere and upper ionosphere [*Khazanov*, 2011]. Also, the formation of these fluxes via MI coupling processes is quite different, compared to the SE energy fluxes presented in Figure 8.

First, note that the thermal fluxes presented in Figure 9 are symmetric for both L shells for the cases All, Nolono, and NoRef12 with respect to the both magnetically conjugated ionospheric regions. This is because the MI coupling conditions for these simulation scenarios are identical with respect to the Northern (1) and Southern (2) Hemispheres. There is a similar mirror symmetry regarding the cases NoRef1 and NoRef2. That is why we only discuss the Northern Hemisphere when interpreting the data presented in Figure 9. Also, inspecting this figure, we note more intense fluxes for $L = 6.8$ than at $L = 4.6$. This is because the secondary electron fluxes responsible for the Coulomb energy deposition into the thermal magnetospheric electrons are more intense for $L = 6.8$ (see Figure 7).

As follows from Figure 9, the scenario in which the conjugate regions are disconnected decreases thermal electron fluxes into both the magnetically conjugate ionospheres. The decrease is bigger in the southern ionosphere, which did not supply any secondary electrons to the magnetosphere. This tendency in the thermal electron flux behavior is consistent with the formation of the total SE energy fluxes presented in Figure 8. However, we have a completely different picture when elastic scattering is absent in the Northern Hemisphere (case NoRef1). Here the thermal fluxes into region 1 increase compared with the run when all processes are taken into account (case All), and this does not correlate with the similar scenario for the formation of total SE energy fluxes. Keeping in mind that most of the secondary electron population, $E < 600$ eV, is responsible for heating the thermal electrons in the magnetosphere, the explanation of the behavior of the thermal electron fluxes is quite simple. When all elastic collisional processes are completely ignored in the Northern Hemisphere, the escaping flux of the secondary electron increases and supplies more energy to the magnetospheric region, thereby heating the thermal electron component.

Ignoring elastic scattering processes in both magnetically conjugate regions (NoRe12) reverses the tendency of the electron thermal flux formation compared to the case of NoRef1. Nevertheless, the intensity of the thermal electron fluxes in this run is larger than that in the All scenario, but less than that discussed above. The reason for this behavior is the complete ignorance of the multiple reflections between the magnetically conjugate points, and, as a result, a decrease in the magnetospheric electrons with energies $E > 600$ eV that are responsible for the production of the secondary electrons (see Figure 7).

5. Summary

This paper should be considered as a continuation of our systematic approach to the formation of the electron distribution function in the regions of the diffuse aurora based on the electron kinetic code STET developed by *Khazanov* [1979, 2011] and by *Khazanov et al.* [2014, 2015a, 2015b]. This particular paper finalizes our MI coupling diffuse aurora studies in the dipole magnetic field geometry. Further work will refocus on the different types of the aurora, as well as on the application of the STET model to study electrodynamical, optical, and energy deposition processes in the coupled MI system.

In the diffuse aurora, precipitating electrons initially injected from the plasma sheet via wave-particle interactions (WPI) degrade in the atmosphere toward lower energies and produce secondary electrons via impact ionization of the neutral atmosphere. These initially precipitating electrons of magnetospheric origin can be additionally reflected back into the magnetosphere by the two magnetically conjugated atmospheres, leading to a series of multiple reflections that can greatly influence the initially precipitating flux at the upper ionospheric boundary (700–800 km). The resultant population of secondary and primary electrons cascade toward the lower energies and escape back to the magnetosphere. Electrons escaping upward from the ionosphere can be trapped in the magnetosphere as they travel inside the loss cone via Coulomb collision with

the cold plasma or by interactions with various plasma waves. Although the scenario described above seems quite obvious, it was *completely* missing in all existing diffuse aurora research.

The idea of the role of MI coupling processes in the formation of diffuse aurora that has been introduced in our previous research by *Khazanov et al.* [2015a, 2015b, 2017] was recently conformed by first optical observations of interhemispheric electron reflections within pulsating aurora by *Samara et al.* [2017]. In this paper they presented ground-based optical signatures of the aurora showing evidence that a certain type of aurora is caused by electrons bouncing back and forth between the two hemispheres. This means that these electrons are responsible for some of the total light in the aurora, a possibility that has largely been ignored in theoretical models and has important implications for our understanding of magnetosphere-ionosphere coupling.

As we demonstrated in this paper, considering only electron precipitation that is driven by ECH and/or whistler waves in the Earth's plasma sheet is not a complete picture, and the MI coupling element in the formation must be taken into account. As shown in this manuscript, WPI processes that drive precipitating fluxes in the region of diffuse aurora from the magnetospheric altitudes are only the first step in the formation of electron precipitation at ionospheric altitudes, and they cannot be separated from the atmospheric "collisional machine" that redistributes and transfers their energy inside the MI coupling system.

References

Hardy, D. A., M. S. Gussenhoven, and D. Brautigam (1989), A statistical model of auroral ion precipitation, *J. Geophys. Res.*, *94*, 370–392, doi:10.1029/JA094iA01p00370.

Horne, R. B., R. M. Thorne, N. P. Meredith, and R. R. Anderson (2003), Diffuse auroral electron scattering by electron cyclotron harmonic and whistler mode waves during an isolated substorm, *J. Geophys. Res.*, *108*(A7), 1290, doi:10.1029/2002JA009736.

Kennel, C. F., and H. E. Petschek (1966), Limit on stably trapped particle fluxes, *J. Geophys. Res.*, *71*, 1–28, doi:10.1029/JZ071i001p00001.

Khazanov, G. V. (1979), The kinetics of the electron plasma component of the upper atmosphereNauka, Moscow, English Translation: Washington, D. C., National Translation Center 80-50707, 1980.

Khazanov, G., M. W. Liemohn, T. I. Gombosi, and A. F. Nagy (1993), Non-steady-state transport of superthermal electrons in the plasmasphere, *Geophys. Res. Lett.*, *20*, 2821–2824, doi:10.1029/93GL03121.

Khazanov, G., and M. W. Liemohn (1995), Nonsteady state ionosphere-plasmasphere coupling of superthermal electrons, *J. Geophys. Res.*, *100*, 9669–9681, doi:10.1029/95JA00526.

Khazanov, G., T. E. Moore, M. W. Liemohn, V. K. Jordanova, and M.-C. Fok (1996), Global collisional model of high-energy photoelectrons, *Geophys. Res. Lett.*, *23*, 331–334, doi:10.1029/96GL00148.

Khazanov, G. V., M. W. Liemohn, E. N. Krivorutsky, J. U. Kozyra, and B. E. Gilchrist (1999), Interhemispheric transport of relativistic electron beams, *Geophys. Res. Lett.*, *26*, 581–584, doi:10.1029/1999GL900045.

Khazanov, G. V. (2011) *Kinetic Theory of Inner Magnetospheric Plasma*, vol. 372, p. 584, Springer, New York.

Khazanov, G. V., A. Glocer, and E. W. Himwich (2014), Magnetosphere-ionosphere energy interchange in the electron diffuse aurora, *J. Geophys. Res. Space Physics*, *119*, 171–184, doi:10.1002/2013JA019325.

Khazanov, G. V., E. W. Himwich, A. Glocer, and D. Sibeck (2015a), The role of multiple atmospheric reflections in the formation of the electron distribution function in the diffuse aurora region, in *Auroral Dynamics and Space Weather*, *AGU Monogr.*, vol. 215, edited by Y. Zhang and L. J. Paxton, pp. 115–130, John Wiley, Hoboken, N. J., doi:10.1002/9781118978719.

Khazanov, G. V., A. K. Tripathi, D. Sibeck, E. Himwich, A. Glocer, and R. P. Singhal (2015b), Electron distribution function formation in regions of diffuse aurora, *J. Geophys. Res. Space Physics*, *120*, 1–25, doi:10.1002/2015JA021728.

Khazanov, G. V., D. G. Sibeck, and E. Zesta (2017), Is diffuse aurora driven from above or below?, *Geophys. Res. Lett.*, *44*, 641–647, doi:10.1002/2016GL072063.

Li, W., B. Ni, R. M. Thorne, J. Bortnik, J. C. Green, C. A. Kletzing, W. S. Kurth, and G. B. Hospodarsky (2013), Constructing the global distribution of chorus wave intensity using measurements of electrons by the POES satellites and waves by the Van Allen Probes, *Geophys. Res. Lett.*, *40*, 4526–4532, doi:10.1002/grl.50920.

Meredith, N. P., A. D. Johnstone, S. Szita, R. B. Horne, and R. R. Anderson (1999), "Pancake" electron distributions in the outer radiation belts, *J. Geophys. Res.*, *104*, 12,431–12,444, doi:10.1029/1998JA900083.

Meredith, N. P., R. B. Horne, R. M. Thorne, and R. R. Anderson (2009), Survey of upper band chorus and ECH waves: Implications for the diffuse aurora, *J. Geophys. Res.*, *114*, A07218, doi:10.1029/2009JA014230.

Newell, P. T., T. Sotirelis, and S. Wing (2009), Diffuse, monoenergetic, and broadband aurora: The global precipitation budget, *J. Geophys. Res.*, *114*, A09207, doi:10.1029/2009JA014326.

Ni, B., R. M. Thorne, R. B. Horne, N. P. Meredith, Y. Y. Shprits, L. Chen, and W. Li (2011a), Resonant scattering of plasma sheet electrons leading to diffuse auroral precipitation: 1. Evaluation for electrostatic electron cyclotron harmonic waves, *J. Geophys. Res.*, *116*, A04218, doi:10.1029/2010JA016232.

Ni, B., R. M. Thorne, N. P. Meredith, R. B. Horne, and Y. Y. Shprits (2011b), Resonant scattering of plasma sheet electrons leading to diffuse auroral precipitation: 2 Evaluation for whistler mode chorus waves, *J. Geophys. Res.*, *116*, A04219, doi:10.1029/2010JA016233.

Petrinec, S. M., D. L. Chenette, J. Mobilia, M. A. Rinaldi, and W. L. Imhof (1999), Statistical X ray auroral emissions–PIXIE observations, *Geophys. Res. Lett.*, *26*(11), 1565–1568, doi:10.1029/1999GL900295.

Rees, D. (1989), *Physics and Chemistry of the Upper Atmosphere*, Cambridge Univ. Press, New York.

Runov, A., V. Angelopoulos, C. Gabrielse, J. Liu, D. L. Turner, and X. Z. Zhou (2015), Average thermodynamic and spectral properties of plasma in and around dipolarizing flux bundles, *J. Geophys. Res. Space Physics*, *120*, 4369–4383, doi:10.1002/2015JA021166.

Samara, M., R. Michell, and G. V. Khazanov (2017), First optical observations of inter-hemispheric electron reflections within pulsating aurora, *Geophys. Res. Lett.*, doi:10.1002/2017GL072794.

Sato, N., A. Kadokura, T. Motoba, K. Hosokawa, G. Björnsson and T. Saemundsson (2016), Interhemispheric symmetries and asymmetries of aurora from ground-based conjugate observations, in *Auroral Dynamics and Space Weather*, *AGU Monogr.*, vol. 215, edited by Y. Zhang and L. J. Paxton, pp. 145–161, John Wiley, Hoboken, N. J., doi:10.1002/9781118978719.

Su, Z., H. Zheng, and S. Wang (2009), Evolution of electron pitch angle distribution due to interactions with whistler mode chorus following substorm injections, *J. Geophys. Res.*, *114*, A08202, doi:10.1029/2009JA014269.

Su, Z., H. Zheng, and S. Wang (2010), A parametric study on the diffuse auroral precipitation by resonant interaction with whistler mode chorus, *J. Geophys. Res.*, *115*, A05219, doi:10.1029/2009JA014759.

Thorne, R. M., B. Ni, X. Tao, R. B. Horne, and N. P. Meredith (2010), Scattering by chorus waves as the dominant cause of diffuse auroral precipitation, *Nature*, *467*, 943–946.

Tripathi, A. K., R. P. Singhal, G. V. Khazanov, and L. A. Avanov (2016), Banded structures in electron pitch angle diffusion coefficients from resonant wave-particle interactions, *Phys. Plasmas*, *23*, 042101, doi:10.1063/1.4944920.